



HAL
open science

Self-interacting dark matter and the delay of supermassive black hole growth

A. Cruz, A. Pontzen, M. Volonteri, T.R. Quinn, M. Tremmel, A.M. Brooks,
N.N. Sanchez, F. Munshi, A. Di Cintio

► **To cite this version:**

A. Cruz, A. Pontzen, M. Volonteri, T.R. Quinn, M. Tremmel, et al.. Self-interacting dark matter and the delay of supermassive black hole growth. *Monthly Notices of the Royal Astronomical Society*, 2020, 500 (2), pp.2177-2187. 10.1093/mnras/staa3389 . hal-02572600

HAL Id: hal-02572600

<https://hal.science/hal-02572600>

Submitted on 25 Aug 2022

HAL is a multi-disciplinary open access archive for the deposit and dissemination of scientific research documents, whether they are published or not. The documents may come from teaching and research institutions in France or abroad, or from public or private research centers.

L'archive ouverte pluridisciplinaire **HAL**, est destinée au dépôt et à la diffusion de documents scientifiques de niveau recherche, publiés ou non, émanant des établissements d'enseignement et de recherche français ou étrangers, des laboratoires publics ou privés.

Self-interacting dark matter and the delay of supermassive black hole growth

A. Cruz,¹★† A. Pontzen,² M. Volonteri,³ T. R. Quinn,⁴ M. Tremmel⁵,⁵ A. M. Brooks,⁶ N. N. Sanchez,⁴ F. Munshi⁷ and A. Di Cintio^{8,9}

¹Department of Physics, University of Washington, Seattle, WA, 98195, USA

²Department of Physics and Astronomy, University College London, 132 Hampstead Road, London NW1 2PS, UK

³Institut d'astrophysique de Paris, 98bis Boulevard Arago, F-75014 Paris, France

⁴Department of Astronomy, University of Washington, Seattle, WA, 98195, USA

⁵Yale Center for Astronomy and Astrophysics, Physics Department, PO Box 208120, New Haven, CT 06520, USA

⁶Department of Physics and Astronomy, Rutgers, The State University of New Jersey, 136 Frelinghuysen Rd. Piscataway, NJ 08854, USA

⁷Department of Physics and Astronomy, University of Oklahoma, 440 W. Brooks St., Norman, OK 73019, USA

⁸Instituto de Astrofísica de Canarias, Calle Via Láctea s/n, E-38206 La Laguna, Tenerife, Spain

⁹Universidad de La Laguna, Avda. Astrofísico Fco. Sánchez, E-38208 La Laguna, Tenerife, Spain

Accepted 2020 October 14. Received 2020 September 22; in original form 2020 April 7

ABSTRACT

Using cosmological hydrodynamic simulations with physically motivated models of supermassive black hole (SMBH) formation and growth, we compare the assembly of Milky Way-mass ($M_{\text{vir}} \approx 7 \times 10^{11} M_{\odot}$ at $z = 0$) galaxies in cold dark matter (CDM) and self-interacting dark matter (SIDM) models. Our SIDM model adopts a constant cross-section of $1 \text{ cm}^2 \text{ g}^{-1}$. We find that SMBH formation is suppressed in the early Universe due to SIDM interactions. SMBH–SMBH mergers are also suppressed in SIDM as a consequence of the lower number of SMBHs formed. Lack of initial merger-driven SMBH growth in turn delays SMBH growth by billions of years in SIDM compared to CDM. Further, we find that this delayed growth suppresses SMBH accretion in the largest progenitors of the main SIDM galaxies during the first 5 Gyr of their evolution. Nonetheless, by $z = 0.8$ the CDM and SIDM SMBH masses differ only by around 0.2 dex, so that both remain compatible with the $M_{\text{BH}}-M_{*}$ relation. We show that the reduced accretion causes the SIDM SMBHs to less aggressively regulate star formation in their host galaxies than their CDM counterparts, resulting in a factor of 3 or more stars being produced over the lifetime of the SIDM galaxies compared to the CDM galaxies. Our results highlight a new way in which SIDM can affect the growth and merger history of SMBHs and ultimately give rise to very different galaxy evolution compared to the classic CDM model.

Key words: black hole physics – hydrodynamics – galaxies: formation – galaxies: star formation – dark matter.

1 INTRODUCTION

The favoured model for dark matter (DM) has long been cold DM (CDM), a single, collision-less particle species with negligible primordial thermal dispersion. Although DM-only simulations of Λ CDM cosmology prove to be very successful on large scales, they predict high central DM density ‘cusps’ (Navarro, Frenk & White 1997; Moore et al. 1998; Bullock et al. 2001; Wechsler et al. 2002), directly in conflict with observations of dwarf irregulars (Flores & Primack 1994; Moore 1994; de Blok & McGaugh 1997), low surface brightness galaxies (de Blok et al. 2001; Kuzio de Naray, McGaugh & de Blok 2008; Kuzio de Naray & Spekkens 2011), nearby field dwarfs (de Blok et al. 2008; Oh et al. 2008), low-mass spiral galaxies (Gentile et al. 2004; Simon et al. 2005; Castignani et al. 2012; Adams et al. 2014), and satellite dwarfs of the Milky Way (MW) (Walker & Peñarrubia 2011; Salucci et al. 2012; Breddels et al.

2013). These observations suggest the existence of kpc-scale DM cores, a discrepancy with Λ CDM known as the core-cusp problem. Spergel & Steinhardt (2000) were among the first to point out that dark matter self-interactions with a mean free path ranging from 1 kpc to 1 Mpc would naturally impact galaxies and clusters of galaxies, while simultaneously preserving the large scale success of Λ CDM. Thus, self-interacting DM (SIDM) was proposed to address the core-cusp problem over a decade ago (Burkert 2000; Spergel & Steinhardt 2000) as it naturally produces cored profiles in the inner 1 kpc of DM haloes in DM-only simulation, which better agree with observations.

On the other hand, it has since been shown that baryonic physics can also create DM cores. In particular, a number of studies show that outflows driven by supernovae (SNe) cause the formation of shallow DM density profiles at the centres of galaxies (Read & Gilmore 2005; Governato et al. 2012; Pontzen & Governato 2012; Brooks & Zolotov 2014; Di Cintio et al. 2014a, b; Pontzen & Governato 2014; Oñorbe et al. 2015; Tollet et al. 2016; Benítez-Llambay et al. 2019). Moreover, high resolution cosmological simulations which include baryonic physics have been shown to produce DM distributions in

* E-mail: admacruz@uw.edu

† National Science Foundation Graduate Research Fellow.

the central regions of dwarfs, which agree well with observations, in CDM and SIDM models (Bastidas Fry et al. 2015, hereafter BF15). This indicates that (1) SIDM and CDM both remain viable DM candidates and (2) baryonic physics in simulations is required to make reliable predictions about the nature of DM.

Despite the successes of simulations of CDM with baryons, degeneracies in baryonic and DM physics still exist given the relatively large uncertainty in subgrid models (see for example Vogelsberger et al. 2014; Robles et al. 2017). Beyond this, they fail to simultaneously produce the densest galaxies observed (Santos-Santos et al. 2018). This seems to be true even for the highest resolution simulations which should be able to reproduce the compactness observed in some galaxies (Garrison-Kimmel et al. 2019). Meanwhile, a series of works have demonstrated that a SIDM model with an interaction cross-section of $\sim 3 \text{ cm}^2 \text{ g}^{-1}$ can reproduce galaxy rotation curves from ~ 50 to 300 km s^{-1} (Kamada et al. 2017; Kaplinghat, Ren & Yu 2019a; Ren et al. 2019), although this is still being debated (Santos-Santos et al. 2020). SIDM also produces a trend in central density of MW-satellites as a function of orbital pericentre (Kahlhoefer et al. 2019; Nishikawa, Boddy & Kaplinghat 2019) which agrees extremely well with *Gaia* data (Kaplinghat, Valli & Yu 2019b) and has not been found in CDM simulations with baryons. These results emphasize that SIDM is becoming an increasingly interesting DM candidate.

However, few cosmological simulations with baryons and SIDM exist to date with most work focusing on dwarf galaxies given the tensions with observations at this mass scale. Vogelsberger et al. (2016) examined MW-mass simulations of SIDM with a single DM particle which was allowed to interact with itself and with a mass-less neutrino-like fermion (dark radiation) but did not include baryons. More recently Di Cintio et al. (2017) compared MW-mass galaxies, as well as lower mass galaxies, from cosmological volumes with side lengths of 8 Mpc in CDM and SIDM with an interaction cross-section of $10 \text{ cm}^2 \text{ g}^{-1}$ and found that at low- z the most massive SIDM SMBHs in galaxies were routinely off-centre from their hosts unlike the CDM SMBHs which remained at their hosts centre.

In this paper, we expand on the work of Di Cintio et al. (2017) by using simulations with baryonic physics and physically motivated models of SMBH formation and growth through mergers (Tremmel et al. 2015, hereafter T15) and accretion (Tremmel et al. 2017, hereafter T17) to study the effects SIDM has on the formation and evolution of SMBHs and their MW-mass host galaxies. MW-mass galaxies are a particularly interesting place to examine SIDM's effect on SMBH growth because these galaxies may or may not be quenched and straddle the regime where SMBHs start to suppress star formation. Unlike Di Cintio et al. (2017) we used a much lower SIDM cross-section of $1 \text{ cm}^2 \text{ g}^{-1}$ and examined SMBH formation and the temporal evolution of SMBHs and their host galaxies in CDM and SIDM cosmologies, starting from high- z . This is important given that the early Universe is much denser than today, and thus the SIDM interaction rate peaks at high- z (Robertson et al. 2015). Still more, in the early Universe the formation of DM cores due to bursty SNe feedback detailed in BF15 are not present for the galaxies we considered given that they have stellar masses less-than or equal to $10^6 M_\odot$, the threshold for star formation to start to core DM haloes (see fig. 7 of Governato et al. 2015). Thus the distinct effects of SIDM are preserved.

The organization of this paper is as follows: in Section 2 we will detail the physics integrated into our suite of simulations. Section 3 will detail our results with a discussion of differences in CDM versus SIDM cosmologies, including star formation and gas content 3.1, SMBH formation 3.2, and eventual growth through mergers and

accretion 3.3. In Section 4, we will discuss the implications of our study as well as summarize and conclude the paper.

2 SIMULATIONS

The simulations examined in this paper were run in a fully cosmological context to $z = 0$. However, this paper will focus on the evolution from $z = 20$ to $z \approx 0.8$, as this time interval is where we see the biggest differences in SMBH growth and star formation in the CDM versus SIDM runs. Furthermore all simulated zoom-in galaxies quench near or at $z \approx 0.8$, and remain quiescent for billions of years. Further, all galaxies have formed $\gtrsim 90$ per cent of their total stellar mass by $z \approx 0.8$.

The simulations were run using Charm N -body GrAvity Solver (CHANGA¹), a smoothed particle hydrodynamics (SPH) N -body tree code (Menon et al. 2015). CHANGA is a successor of GASOLINE and thus includes the same models for low temperature metal line cooling, self-shielding, star formation (using a Kroupa 2001, IMF), ‘blastwave’ SNe feedback, and cosmic UV background (Wadsley, Stadel & Quinn 2004; Stinson et al. 2006; Wadsley, Veeravalli & Couchman 2008). The SPH implementation also includes thermal diffusion (Shen, Wadsley & Stinson 2010) and eliminates artificial gas surface tension by using a geometric mean density in the SPH force expression (Ritchie & Thomas 2001; Governato et al. 2015; Menon et al. 2015; Wadsley, Keller & Quinn 2017). This addition better simulates shearing flows with Kelvin–Helmholtz instabilities.

In all simulations we assumed a Λ dominated cosmology ($\Omega_m = 0.3086$, $\Omega_\Lambda = 0.6914$, $h = 0.67$, $\sigma_8 = 0.77$; Planck Collaboration XVI 2014) and used the ‘zoom-in’ methods described by Pontzen et al. (2008). All simulations are run with a Plummer equivalent softening length, $\epsilon = 250 \text{ pc}$ and mass resolution of $1.4 \times 10^5 M_\odot$ and $2.1 \times 10^5 M_\odot$ for DM and gas particles, respectively. We used two DM models: the standard CDM model and an SIDM model with a constant interaction cross-section of $\sigma_{\text{dm}} = 1 \text{ cm}^2 \text{ g}^{-1}$. We re-simulate two of the MW-mass galaxies ($M_{\text{vir}} \approx 7 \times 10^{11} M_\odot$ at $z = 0$, see equation 1) presented in Sanchez et al. (2019) with SIDM (their GM2 and GM3 galaxies). As the GM moniker suggests, these galaxies are part of a series constructed using ‘genetic modification’ (Roth, Pontzen & Peiris 2016), in the case of GM2 and GM3 this allows us to robustly test the effects of SIDM on SMBH formation and subsequently, star formation. Specifically, we simulated GM3 (which has quenched star formation) in order to examine strong effects of SMBHs, which play a large role in quenching galaxies (Pontzen et al. 2017). GM2 (also quenched) allows us to check for sensitivity to small changes. The GM runs considered have almost identical histories but differ due to an altered satellite population, which results in a different rate of accretion at early times; for more information see Sanchez et al. (2019). Our use of GM2 and GM3 allows us to specifically verify that our SIDM results are robust to this aspect of the assembly of a halo. In this paper, we use the same nomenclature as Sanchez et al. (2019) for the CDM galaxies, i.e., GM2, GM3, and append ‘S11’ (i.e. GM3S11, etc.) for the counterpart simulations run with SIDM with an interaction cross-section of $\sigma_{\text{dm}} = 1 \text{ cm}^2 \text{ g}^{-1}$.

After running our simulations we extract all of our main haloes and sub-haloes using the AMIGA halo finder (Knollmann & Knebe 2009). We calculate the virial mass of haloes as

$$M_{\text{vir}} = \frac{4}{3} \pi \Delta_h \bar{\rho} R_{\text{vir}}^3, \quad (1)$$

¹www-hpcc.astro.washington.edu/tools/changa.html

where $\bar{\rho}$ is the critical density of the Universe, $\Delta_h = 200$ is the overdensity threshold, and R_{vir} is the halo virial radius.

2.1 Self-interacting dark matter physics

The SIDM implementation used in our simulations closely follows the standard Monte Carlo method described in detail in BF15. We briefly describe the features of this model here and refer the reader to BF15 and references therein for details. SIDM interactions are modelled under the assumption that each simulated DM particle represents a patch of DM phase-space density and that the probability of collisions is derived from the collision term in the Boltzmann equation. Collisions are elastic and explicitly conserve energy and momentum. When a particle collision is detected, particles are isotropically and elastically scattered to random angles. For a detailed discussion see also Rocha et al. (2013) and Koda & Shapiro (2011), Yoshida et al. (2000), D’Onghia & Burkert (2003), Vogelsberger, Zavala & Loeb (2012), Kaplinghat et al. (2014). The SIDM interaction rate of particles will vary with local DM density $\rho_{\text{dm}}(r, z)$, cross-section σ_{dm} , and velocity dispersion $v(r, z)$ as

$$\Gamma_{\text{SI}}(r, z) \simeq \rho_{\text{dm}}(r, z)v(r, z)\sigma_{\text{dm}} \quad (2)$$

up to an $\mathcal{O}(1)$ constant (Rocha et al. 2013). Collisions between SIDM particles result in energy exchange, which heat the halo centre until it becomes isothermal (Balberg, Shapiro & Inagaki 2002; Colín et al. 2002; Koda & Shapiro 2011).

The SIDM cross-section σ_{dm} must adhere to several astrophysical observations, including the necessity of forming DM cores in faint galaxies without the over-evaporation of MW-mass galaxy satellites or galaxies in clusters and maintaining the elliptical shape of haloes and clusters (Firmani et al. 2001; Gnedin & Ostriker 2001; Peter et al. 2013; Robertson, Massey & Eke 2017). Utilizing SIDM-only simulations with these observations in mind, authors have found the relevant range to impact galaxy evolution and avoid upper limits to be $0.1 \text{ cm}^2 \text{ g}^{-1} < \sigma_{\text{dm}} < 1 \text{ cm}^2 \text{ g}^{-1}$ for velocity-independent cross-sections (Vogelsberger et al. 2012; Peter et al. 2013; Rocha et al. 2013; Vogelsberger & Zavala 2013; Zavala, Vogelsberger & Walker 2013; Cyr-Racine et al. 2016; Vogelsberger et al. 2016). A velocity-dependent cross-section could ease the constraints on σ_{dm} by allowing DM to behave as a collisional fluid on the scale of dwarfs, and more collision-less at the scale of clusters (Yoshida et al. 2000; Colín et al. 2002; Elbert et al. 2018). Velocity-dependent cross-sections can also influence when the SIDM interaction rate peaks as a function of redshift (Robertson et al. 2015). Further, a velocity-dependent cross-section allows for a value of $3 \text{ cm}^2 \text{ g}^{-1}$ in the range of rotational velocities explored in Ren et al. (2019) and Kaplinghat et al. (2019a). Beyond the development of the gravothermal catastrophe of SIDM haloes, very large cross-sections at dwarf scales are in principle not ruled out. Velocity-dependent cross-sections with large values at dwarf scales produce distinct circular velocity profiles of the lowest mass galaxies compared to the constant cross-section model (Zavala et al. 2019). The interaction cross-section σ_{dm} for all SIDM runs in this work was set to $1 \text{ cm}^2 \text{ g}^{-1}$.

2.2 Star formation

Since this paper is largely focused on star formation, we review here in more detail the star formation prescription (Stinson et al. 2006) and parameters (T17) used in our simulations.

Gas particles are allowed to form stars in our simulations if they surpass minimum density (n_*) and maximum temperature (T_*) thresholds. The probability of creating a star particle from gas

with dynamical time t_{dyn} and characteristic star formation time, Δt , assumed to be 10^6 yr is given as

$$p = \frac{m_{\text{gas}}}{m_{\text{star}}} (1 - e^{-c_* \Delta t / t_{\text{dyn}}}), \quad (3)$$

where c_* is the star formation efficiency. Further, star formation is regulated by the fraction of SNe energy that is coupled to the ISM, our star formation efficiency (c_*), and our density and temperature thresholds. The values we have adopted for our sub-grid parameters are as follows:

- (i) star formation efficiency $c_* = 0.15$
- (ii) Gas density threshold, $n_* = 0.2 \text{ cm}^{-3}$
- (iii) Gas temperature threshold, $T_* = 10^4 \text{ K}$
- (iv) SNe energy coupling efficiency, ϵ_{SN} of 75 per cent

SNe feedback adopts a ‘blastwave’ implementation (Stinson et al. 2006) and gas cooling is regulated by metal abundance as in Guedes et al. (2011).

2.3 Black hole physics

Our simulations also include SMBH formation and improved SMBH accretion and feedback models which explicitly follows the orbital evolution of SMBHs (T15; T17).

The SMBH seed (with seed mass of $10^6 M_{\odot}$) formation is connected to the physical state of the gas in the simulation at high- z , without assumptions about the halo occupation fraction. SMBHs seeds form in the early universe if the gas particle has already met the star formation thresholds (see Section 2.2) and additionally has

- (i) Low metallicity ($Z < 3 \times 10^{-4}$)
- (ii) Density 15 times that of the star formation threshold (3 cm^{-3})
- (iii) Temperature between 9500 and 10 000 K

This seeding method allows SMBHs to naturally populate galaxies of different masses. Seed SMBH formation is limited to the highest density peaks in the early Universe with high Jeans masses and to gas that is cooling relatively slowly, thus approximating SMBH formation sites with those predicted for SMBH seed formation (Volonteri 2012). This seeding method forms most SMBH seeds within the first Gyr of the simulation, which allows us to follow SMBH dynamics throughout the assembly of the host halo, even for small haloes.

Another important improvement in the SMBH model utilized in these simulations is the treatment of dynamical friction, the gravitational wake of a massive body moving in the extended potential of a medium, which will cause the orbit of SMBHs to decay towards the centre of massive galaxies (Chandrasekhar 1943; Binney & Tremaine 2008). Previously, authors have used analytic expressions to compute the dynamical friction time-scale t_{df} of rigid bodies merging in the centre of galaxies (i.e. Taffoni et al. 2003; Boylan-Kolchin, Ma & Quataert 2008), demonstrating that this time-scale can easily exceed several Gyr (Di Matteo, Springel & Hernquist 2005; Sijacki et al. 2007; Schaye et al. 2015). The advection technique repositions and forces SMBHs to the galaxy centre during merger events or during satellite accretion, and therefore lacks realistic sinking time-scales for SMBHs within galaxies. In this work, we instead use a prescription of dynamical friction which explicitly follows the orbital evolution of SMBHs, introduced by T15. This prescription utilizes a sub-grid approach for modelling unresolved dynamical friction on scales smaller than our gravitational softening length, adding a force correction to the SMBH acceleration. The SMBH then experiences

a dynamical friction force according to

$$\mathbf{F}_{\text{df}} = -4\pi G^2 M_{\text{BH}} \rho_{\text{host}}(< v_{\text{BH}}) \ln(\Lambda) \frac{v_{\text{BH}}}{v_{\text{BH}}^3}, \quad (4)$$

where M_{BH} is the mass of the SMBH, v_{BH} is the speed of the SMBH relative to the local centre of mass velocity, $\rho_{\text{host}}(< v_{\text{BH}})$ is the density of the host background particles with velocities less than the v_{BH} . The Coulomb logarithm, $\ln(\Lambda)$, depends on the minimum and maximum impact parameters such that $\ln(\Lambda) \sim \ln(b_{\text{max}}/b_{\text{min}})$. Given that dynamical friction is well resolved at scales above a softening length we take the maximum impact parameter, $b_{\text{max}} \sim \epsilon$ to avoid double counting. The minimum impact parameter, b_{min} , is taken to be the minimum 90° deflection radius with a lower limit set to be the Schwarzschild radius (see T15 for more details). This acceleration from equation (4) is added to the SMBH's current acceleration and integrated in the following time-step. The resulting sinking time-scale t_{df} will thus be dependent on the density of the surrounding galaxy, and on the mass and velocity of the SMBH itself. T15 showed that this technique produces realistically sinking SMBHs. Correctly accounting for this time-scale can lead to SMBH pairs that exist at kpc-scale separations for several Gyr (Tremmel et al. 2018a). In CDM simulations, it is possible to have ‘wandering’ SMBHs with sinking time-scales longer than a Hubble time (Bellovary et al. 2010, 2019; Tremmel et al. 2018b), an effect that can be exacerbated by the lower central densities caused by SIDM (Di Cintio et al. 2017).

The SMBHs in our simulation also obey a modified Bondi–Hoyle accretion which accounts for the rotational support of the surrounding gas. Our SMBHs accrete according to T17:

$$\dot{M}_{\text{BH}} = \alpha \pi (GM_{\text{BH}})^2 \rho \times \begin{cases} \frac{1}{(v_{\text{bulk}}^2 + c_s^2)^{3/2}} & v_{\text{bulk}} > v_\theta \\ \frac{c_s}{(v_\theta^2 + c_s^2)^2} & v_{\text{bulk}} < v_\theta \end{cases}, \quad (5)$$

$$\alpha = \begin{cases} \left(\frac{n}{n_*}\right)^\beta & n \geq n_* \\ 1 & n < n_* \end{cases}$$

where ρ is the local gas density, and c_s is the sound speed of the gas. Values for density and temperature of nearby gas are estimated from smoothing over the 32 nearest gas particles and accretion is not allowed to occur from gas particles farther than $4 \times \epsilon$. The tangential velocity, v_θ , is derived from the resolved kinematics of nearby gas particles and compared to v_{bulk} , the overall bulk motion of the gas. When either the bulk motion or internal energy of the gas dominates over rotational motion, the accretion model converges to the Bondi–Hoyle prescription. In either case, we add a boost factor, α , calculated by comparing the density of nearby gas particles to our star formation density threshold. This is considered to be the threshold beyond which our simulation no longer fully resolves the internal structure of gas. For lower densities, we assume that the gas is not sufficiently multiphase to require such a boost, as in Booth & Schaye (2009). How much this boost increases with density is governed by β , a free parameter, which is set to 2, as is discussed in section 5.5 of T17. This accretion prescription will thus naturally limit accretion of SMBHs that form in unfavourable environments such as in dwarf galaxies.

Energy from accretion is then isotropically transferred to nearby gas particles with a technique similar to the blast wave SNe feedback of Stinson et al. (2006); i.e. gas cooling is turned off for the gas particles immediately surrounding the SMBH, which resembles the continuous transfer of energy during each SMBH time-step.

This cooling shut off is only for a single BH time-step (typically 10^4 – 10^5 yr) and has been shown to result in large scale outflows that can quench star formation in massive galaxies and enrich the circumgalactic medium (Pontzen et al. 2017; Sanchez et al. 2019; Tremmel et al. 2019). The rate at which energy is coupled to the surrounding gas particles is given by,

$$\dot{E}_{\text{BH}} = \epsilon_r \epsilon_f \dot{M}_{\text{BH}} c^2, \quad (6)$$

where \dot{M}_{BH} is the accretion rate defined in equation (5) and $\epsilon_r = 0.1$ and $\epsilon_f = 0.02$ are the radiative and feedback efficiencies, respectively, and c is the speed of light.

It should be noted that the sub-grid parameters used in this work to regulate star formation and feedback from SMBHs and SNe were optimized against a comprehensive set of $z = 0$ Λ CDM galaxy scaling relations using a multidimensional parameter search as detailed in T17. It is important to note that the sub-grid physics have in no way been optimized to produce any characteristics at high- z , making all of the high- z evolution of SMBHs in these simulations purely predictions of the simulation. Finally, the SIDM simulations were run with the same subgrid parameters found in T17 which were optimized to a set of Λ CDM simulations. Nevertheless, we find that our SIDM simulations remains compatible with the M_* – M_{BH} relation and thus may not demand re-calibration in SIDM, but it should be noted that this was not known a priori.

3 RESULTS

In this section, we examine the star formation and gas content of CDM versus SIDM simulations, and how gas content is connected to the activity of SMBH and SNe feedback. The formation of SMBHs in CDM and SIDM is considered, as well as the growth of the central SMBH in the largest progenitors of what become the main MW-mass galaxies at $z = 0$. We detail the growth of the central SMBH through mergers and through accretion. Differences in SMBH feedback are then examined along with the connection between SMBH feedback and star formation.

3.1 Star formation and gas content

When comparing star formation histories (SFHs), we include only the most massive progenitors of the main haloes in each simulation at $z = 0$, excluding star formation from satellites. We see stark differences between the SFHs of MW-mass galaxies that clearly depend on the assumed DM physics as illustrated in Fig. 1. The zoom-in simulations with CDM (GM2 and GM3, solid orange and purple curves, respectively) show MW-mass galaxies with relatively stable star formation rates (SFRs) of 5 – $8 M_\odot \text{yr}^{-1}$ over roughly 6 Gyr of cosmic time, whereas those zoom-in simulations that include SIDM (GM2SI1 and GM3SI1, dashed orange and purple curves, respectively) exhibit much higher SFRs and overall burstier SFHs.

The star formation in GM3SI1 starts to deviate from CDM beyond 30 per cent around $t = 3$ Gyr (where t is cosmic time) and beyond 50 per cent starting around $t = 4.5$ Gyr. The ratio between SFR in GM3SI1 to GM3 can be as high as 8.1 near $t \approx 5.5$ Gyr where GM3SI1 goes through a ‘starburst’ period before eventually quenching near $t \approx 6.5$ Gyr. In total, GM3SI1 produces 3.7 times more stars over its lifetime compared to GM3.

The difference in SFH between GM2SI1 and GM2 is slightly less dramatic for the first 4 Gyr of the galaxies’ lifetimes; however GM2 and GM2SI1 start to deviate from one another after $t = 4$ Gyr faster than the galaxies in the GM3-suite runs. The ‘burstiness’ near $t = 5.5$ Gyr is also more enhanced in the GM2SI1 versus GM2 runs

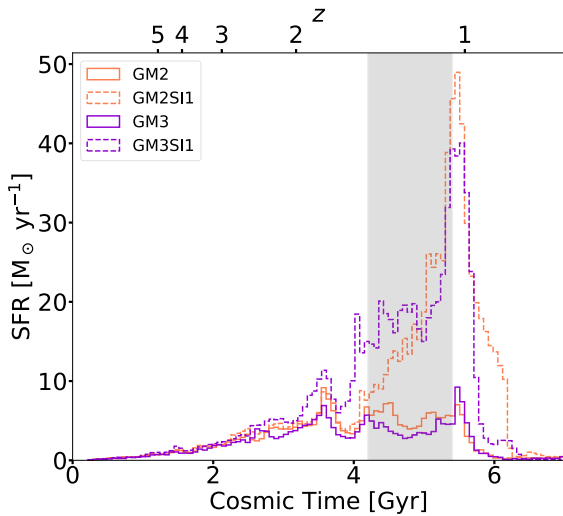


Figure 1. Star formation rate as a function of cosmic time from $t = 0$ – 7 Gyr. There is a striking difference between the GM3 and GM3SI1 runs, as well as in the star formation between GM2 and GM2SI1. The main halo of GM3SI1 ($M_{\text{vir}} \approx 8 \times 10^{11} M_{\odot}$) produces 3.7 times more stars than the CDM GM3 galaxy over its lifetime, but still quenches near 6 Gyr. The GM2SI1 produces 3.1 times more stars compared to GM2 over its lifetime. GM2SI1 starts to quench a bit later (starting near $t = 6.2$ Gyr) compared to GM2, GM3, and GM3SI1. The grey shaded region represents the time interval in which we examine gas content.

Table 1. Galaxy properties at $z = 0.8$.

Sim	M_{vir}^a M_{\odot}	M_*^b M_{\odot}	M_g^c M_{\odot}	M_{BH}^d M_{\odot}	R_{vir}^e kpc
GM2	4.6×10^{11}	1.3×10^{10}	3.9×10^{10}	5.1×10^7	140.8
GM2SI1	5.1×10^{11}	3.6×10^{10}	6.2×10^{10}	4.6×10^7	148.6
GM3	4.5×10^{11}	9.8×10^9	3.5×10^{10}	6.2×10^7	139.2
GM3SI1	5.0×10^{11}	3.6×10^{10}	5.2×10^{10}	4.0×10^7	147.5

Notes.^a Halo virial mass as defined in equation (1).

^b Total stellar mass within R_{vir} .

^c Total gas mass within R_{vir} .

^d Mass of central SMBH in major progenitor of MW-mass galaxies.

^e Halo virial radius, R_{vir} .

compared to the enhancement seen in the GM3-suite runs. The ratio between SFR in GM2SI1 and GM2 can be as high as 8.6. The GM2SI1 galaxy produced 3.1 more stars over its lifetime compared to the GM2 galaxy. Halo mass, stellar mass, and other properties of our galaxies at $z \approx 0.8$ ($t = 7$ Gyr) are detailed in Table 1.

The DM-model-dependent differences seen in the SFHs are also apparent in UVI images of the stars in each galaxy. Each row of Fig. 2 samples a different ‘epoch’ of the SFH and each column shows one of the four simulated galaxies. From bottom to top, the $z = 2.2$ snapshot represents the first epoch, where we see differences of up to 30 per cent in the SFHs of the SIDM galaxies compared to the CDM galaxies. During this epoch, the SIDM galaxies are only slightly brighter than the CDM galaxies. The $z = 1.3$ snapshot samples the second epoch, where the star formation in the SIDM galaxies deviates from the CDM galaxies beyond 50 per cent. In this epoch, the CDM galaxies are irregular, whereas the SIDM galaxies are more spiral and much brighter in their centres. The $z = 1.2$ snapshot represents the epoch just before the ‘starburst’ in the SIDM galaxies. Here, the SIDM galaxies retain their spiral morphology while the CDM galaxies remain irregular. Finally, the $z = 1$ snapshot

represents the epoch when the CDM galaxies quench. In the CDM galaxies the overall surface brightness decreases and the galaxies appear more elliptical whereas the SIDM galaxies surface brightness decreases in the outer regions but remains high in their centres. Thus, examining UVI images of the CDM and SIDM galaxies in each suite demonstrates DM-model-dependent differences in morphology and stellar evolution.

These differences are substantial given that the two sets of simulations come from the exact same ICs, respectively, with only the underlying DM models changing. While Keller et al. (2019) has emphasized that star formation rates can vary stochastically between different runs due to purely numerical artefacts, this is not the cause of our differences here. First, the extent of our differences are vastly higher than those found by Keller et al. (2019) and, secondly, the identical trends seen when switching to SIDM in GM2 and GM3 serves as an independent robustness check. The large difference we see in SFH must be attributable to changes in the properties of the galaxy’s gas. Excess gas that is dense ($n \geq 0.2 m_p / \text{cm}^3$) and cool ($T \leq 10^4$ K) can turn into stars in our simulations. Thus, we next examine the gas content of the SI1 galaxies compared to the CDM galaxies.

In Fig. 3 we examine the gas content within spheres of various cut-off radii, r_c , centred on the shrinking sphere centre (found using methods of Power et al. 2003 implemented in Pontzen et al. 2013) of the most massive progenitors of the main galaxy at $z = 0$ and compare the mass in gas between SIDM and CDM in the GM3-suite. The gas is broken down into hot gas and cold gas, where cold gas is the gas that satisfies our temperature criteria for star formation and hot gas is gas with $T > 10^5$ K. Fig. 3 shows cosmic time between 4.2 and 5.4 Gyr, leading up to the ‘starburst’, or the peak of star formation, in SIDM and after both the CDM and SIDM galaxies undergo mergers. The period of time for which we examine the gas properties is highlighted in grey in Fig. 1. The SFH between the CDM and SIDM galaxies begins to deviate beyond 30 per cent around $t = 3$ Gyr and beyond 50 per cent after $t \approx 4$ Gyr. The deviation accelerates rapidly after this. Thus, this is the time region that is interesting to examine in order to understand the differences in the SFH between the CDM and SIDM galaxies. The ratio of cold and hot gas decreases smoothly as r_c increases, indicating that there is more gas in the inner regions of the SIDM galaxy compared to the CDM galaxy.

In the inner 10 kpc SIDM has much more cold and hot gas compared to CDM. The excess cold gas is responsible for the increased number of stars formed in the SIDM galaxies. The increased number of stars formed in the SIDM galaxies are responsible for the excess hot gas, via increased SNe-feedback (which is proportional to the number of stars formed). Therefore, the excess hot gas in the SIDM galaxies is a consequence of their increased SFRs. More specifically, the ratio of hot gas in SIDM compared to CDM rises with increasing difference in SFR (and therefore SFR feedback), which is seen in the particularly strong increase at the end of the time interval shown in Fig. 3 and at the end of the corresponding shaded region in Fig. 1 where the SFR peaks in SIDM but not in CDM. The excess cold gas can be caused by either stronger inflows to the centre of the SIDM galaxies or cold gas being pushed out and depleted from the inner 10 kpc of CDM galaxies. Lagrangian particle tracking which matches and traces gas particles from the inner 10 kpc of the CDM and SIDM galaxies shows that in CDM galaxies gas that is diffuse at later times was more dense and structured at earlier times. This indicates that gas is being more readily disrupted in the central region in our CDM runs. We show in the next section that this is due to differences in SMBH feedback between the CDM and SIDM simulations.

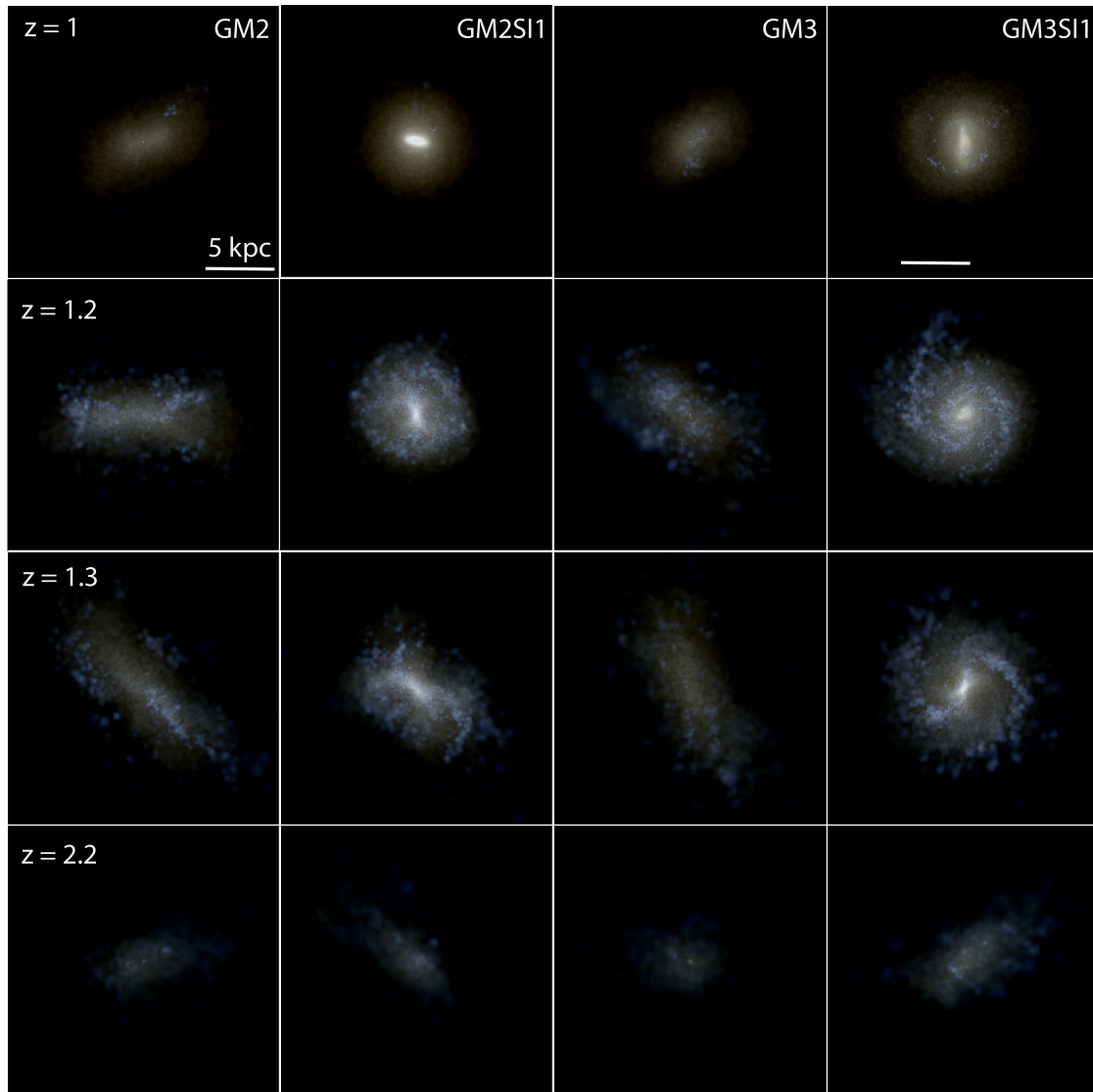


Figure 2. Cosmic evolution of stars in all four galaxies. Four snapshots taken (from the top) at $z = 1, 1.2, 1.3,$ and 2.2 and showing (from left to right) GM2, GM2SI1, GM3, GM3SI1. The stars are shown in UVI colours assuming a Kroupa IMF and are oriented such that the angular momentum axis of the stars calculated from PYNBODY is in the z -direction which points out of the page. All images encompass 20 kpc on each side and the 5 kpc scale (on the upper left) is in physical units. The surface brightness for all images ranges from 23 to $13.6 \text{ mag arcsec}^{-2}$. The four redshift snapshots are chosen to sample four different ‘epochs’ that are present in the SFHs of our galaxies. From bottom up, at $z = 2.2$ GM3SI1 has started to deviate from GM3 in star formation, but GM2SI1 and GM2 remain similar at $z = 2.2$, which is clear in the similar UVI images at this redshift. The $z = 1.3$ snapshot represents an epoch where the star formation in the SIDM galaxies deviate from the CDM galaxies beyond the 50 per cent level; at this redshift the SIDM galaxies are spiral galaxies and their CDM counterparts are irregular. The $z = 1.2$ snapshot represents the epoch near the SIDM galaxies ‘starburst’ period; here the SIDM galaxies retain their spiral morphology while the CDM galaxies remain more irregular. By $z = 1$, the CDM galaxies are quenching and turning red; the SIDM galaxies are also turning red, but remain much brighter in their centres compared to the CDM galaxies.

3.2 Black hole formation

In Fig. 4, we explore the total number of SMBHs formed in our simulations versus cosmic time. SMBHs formation is suppressed in the SIDM runs, when compared to their CDM counterparts. GM3 forms 2.9 times as many SMBHs in the early universe compared to GM3SI1 and GM2 forms 1.7 times as many SMBHs as GM2SI1. Within the first Gyr of our GM3-suite simulations, the GM3 simulation has formed about 2 times as many SMBHs as the GM3SI1 simulation. After 1 Gyr, the GM3 galaxy quickly produces about 10 more SMBHs whereas the GM3SI1 galaxy production flattens out, producing only 1 more SMBH for the remainder of the

simulation. The difference between GM2-suite galaxy simulations are less drastic, which is reflected in differences in star formation. During the first Gyr, SMBH production is similar until near $t = 1 \text{ Gyr}$, where GM2 has produced about 20 SMBHs, compared to GM2SI1 which has produced around 15 SMBHs. After 1 Gyr, the GM2 simulation continues to produce SMBHs, while the GM2SI1 simulation has nearly stopped.

Our SMBH seeding prescription depends on the gas density in haloes in the high- z universe. To determine how the halo densities have affected the formation of the SIDM SMBHs, we look at all redshift snapshots before $z = 6$ and determine the approximate

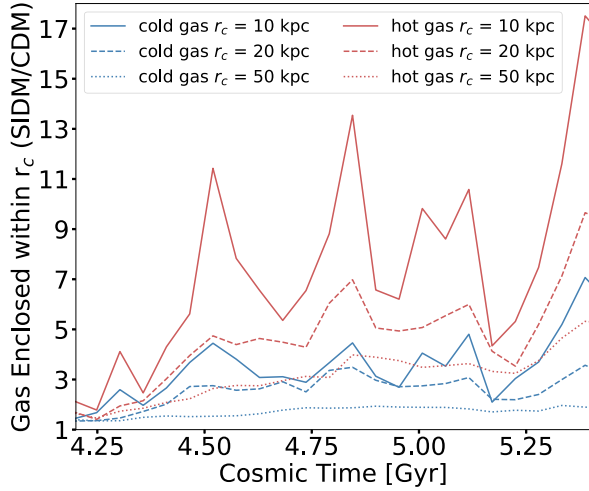


Figure 3. Ratio of GM3S11 gas compared to GM3 gas enclosed within a spherical volume with cut off radius of r_c . Gas content is broken down into hot gas ($T > 10^5$ K) and cold gas, where cold gas is defined to be gas that satisfies our temperature criteria for star formation ($T < 10^4$ K). The hot gas is shown in red where as the cold gas is shown in blue. Various line styles are used to indicate gas in different cut off radii. The ratio of cold gas within the inner 10 kpc comes close to 7 just before the ‘starburst’ near $t \approx 5.5$ Gyr in GM3S11. At every cut off radius the ratio of gas in GM3S11 compared with GM3 is greater than 1 and gradually increases as r_c decreases. We use the GM3-suite as a representative example of both GM suites.

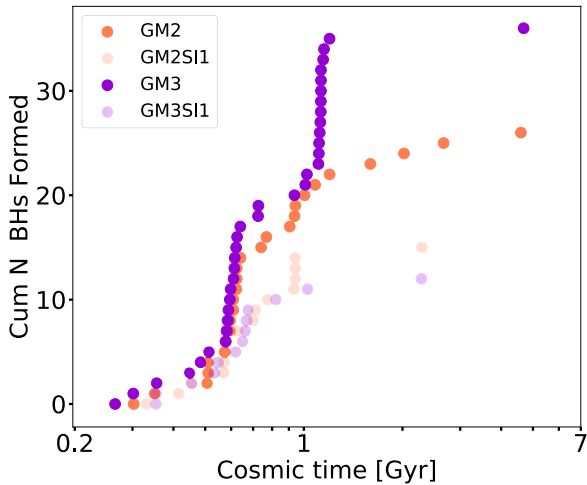


Figure 4. Cumulative number of SMBH seeds versus log of cosmic time. In both the GM2-galaxy and the GM3-galaxy suites the CDM galaxies produce more SMBHs in the first 2 Gyr of the simulation. GM3 produces 2.9 times more SMBHs than GM3S11, where as GM2 produces 1.7 times more SMBHs than GM2S11.

halo mass range in which SMBHs form to be between 10^8 and $10^{10} M_\odot$. For haloes in this mass range we then examine the average gas density within 500 pc of the haloes’ shrinking sphere centre in the $z = 6$ snapshot. This snapshot is the closest in time to peak SMBH production. In Fig. 5 we plot the cumulative probability to have a given average central gas density versus average gas density. We find that the SIDM simulations tend to have higher cumulative probabilities at lower average central gas densities compared to the CDM simulations. We conduct a two-sample Kolmogorov–Smirnov test and determine that in the GM2-suite, the null hypothesis that the

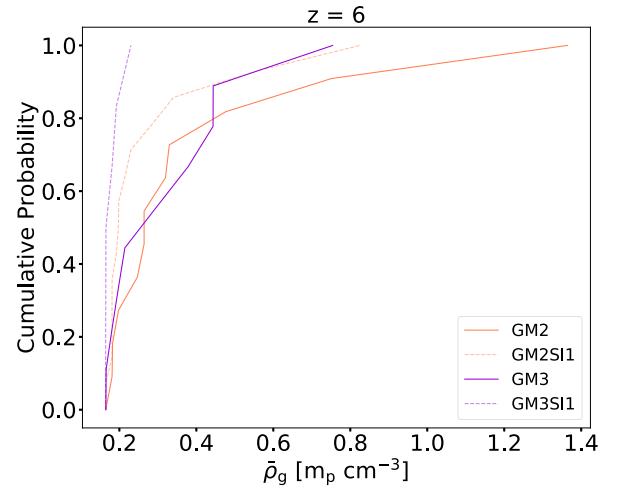


Figure 5. Cumulative probability of central gas density versus average central gas density (gas within 500 pc) for haloes within the mass range for SMBH formation at $z = 6$, the redshift snapshot near ‘peak’ SMBH production in the simulations. The SIDM galaxies have higher cumulative probability of having lower central gas densities compared to the CDM galaxies.

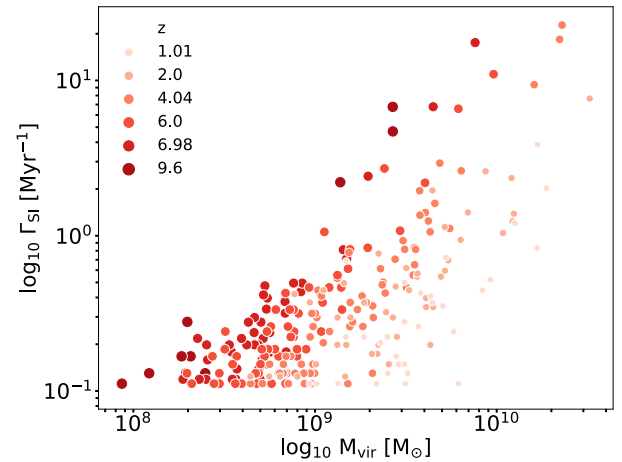


Figure 6. SIDM interaction rate as a function of halo mass at various redshifts. Mass range selected to emphasize halo mass range of SMBH formation sites at $z \gtrsim 6$. At a given mass, the SIDM interaction rate is higher at higher redshift, consistent with the fact the high- z Universe is denser than the low- z Universe.

samples are drawn from the same distribution, is rejected at the 0.24 level. In the GM3-suite the null hypothesis is rejected at the 0.16 level. Further, we find that the DM component dominates the total galaxy density in these haloes, with the baryon density following the DM component (see also Vogelsberger et al. 2014).

To determine the influence of SIDM on DM, and subsequently gas, densities at high- z , we used Lagrangian particle tracing to calculate the average SIDM interaction rate at a given halo mass for a number of redshifts. For each final redshift snapshot, we traced back DM particles to the previous snapshot and calculated the change in the cumulative number of interactions and for each halo. We then found the corresponding time interval between the snapshots and calculated the average interaction rate. In Fig. 6 we plot the total interaction rate versus halo mass at various redshifts. We find that, at a given halo mass, the average SIDM interaction rate increases towards higher

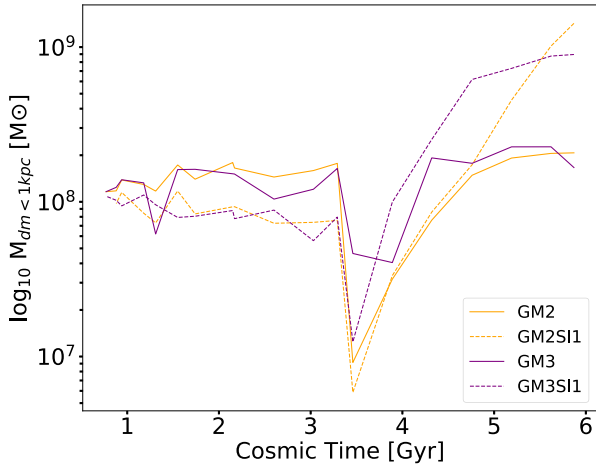


Figure 7. Dark matter mass enclosed in the inner 1 kpc versus cosmic time. At early times the SIDM mass enclosed is almost always below the CDM mass enclosed. Near $t = 3.5$ Gyr all galaxies undergo mergers, which can be seen in the dip in all enclosed mass during this period. At late times, the stars and gas build up in the central regions of the SIDM galaxies, and adiabatic contraction causes the SIDM galaxies to have more DM mass enclosed in the inner 1 kpc.

redshift. This trend as well as the general shapes of our interaction rate as a function of M_{vir} at different redshifts are in agreement with previous analytic work on the cosmic evolution of SIDM interaction rates (see for example the second panel of fig. 1 in Robertson et al. 2015). Further, at $z = 6$, just before the peak of SMBH formation in the CDM galaxies, the SIDM interaction rate is more than an order of magnitude higher than it is at $z = 1$. We attribute this increase to the increasing mean density of the Universe at higher redshift (see equation 2).

Finally, we hypothesize that the decrease in central gas densities and subsequent suppression of SMBH formation is due to the DM component being suppressed in the central region due to DM self-interactions and the baryon density following the DM component. Here we’ve made several measurements to test this: (1) the SIDM interaction rate appears to be sufficient to relax the DM density at high- z , and (2) our measurement of the central gas density is consistent with it being lower in the SIDM simulations due to inner DM mass deficit relative to CDM. Finally, we show this DM mass deficit in Fig. 7. Here we find the largest progenitor of our main $z = 0$ galaxies at earlier times and find the DM mass enclosed within 1 kpc of the progenitors’ shrinking sphere centre. The SIDM mass enclosed within 1 kpc is suppressed relative to the CDM mass enclosed at high redshift. This mass deficit at high redshift causes the cumulative probability of average central gas density to be lower in the SIDM cases relative to the CDM cases, which ultimately gives rise to fewer SMBHs formation sites. At low redshift, the DM mass enclosed is higher in SIDM than in CDM due to adiabatic contraction caused by the build up of stars.

3.3 Black hole mergers and accretion

SMBH–SMBH mergers become more frequent in the early universe in our CDM simulations. This can be seen in the top and bottom panels of Fig. 8. The top panel shows the growth of the most central SMBH in the largest progenitors of our most massive haloes at $z = 0$. This mass increases due to SMBH–SMBH mergers and through our modified Bondi-Hoyle accretion prescription detailed in equation

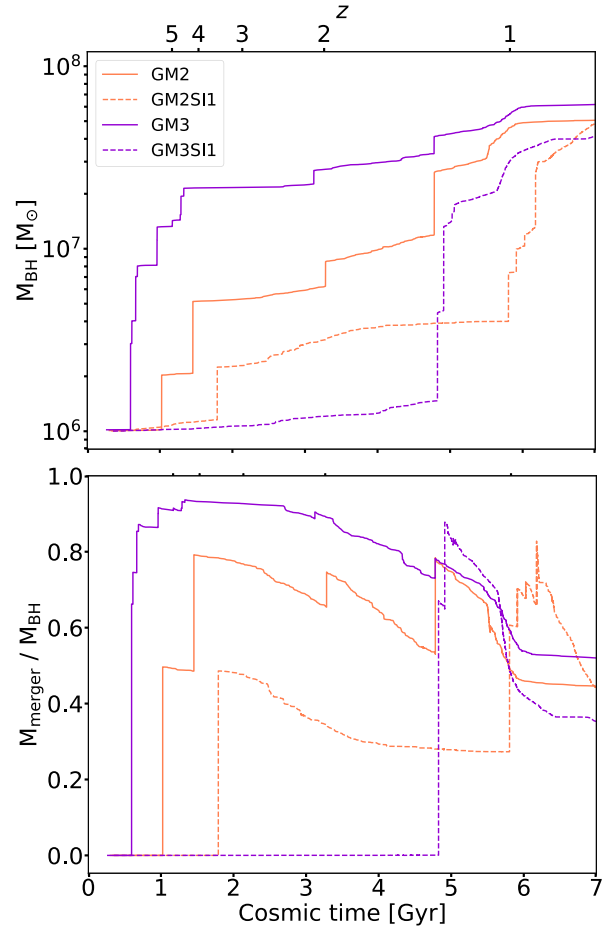


Figure 8. Top panel: Mass of the most massive SMBH as a function of cosmic time in each simulation. In both GM2 and GM3 CDM simulations the SMBHs grow more rapidly through mergers before $t = 2$ Gyr. The increased number of SMBHs in the CDM galaxies will lead to more SMBH–SMBH mergers in the early universe, resulting in enhanced SMBH mass growth through mergers in the first 2 Gyr in the CDM galaxies. This enhanced growth contributes to fast SMBH accretion in the CDM galaxies, given modified Bondi-Hoyle accretion is proportional to M_{BH}^2 . Bottom panel: BH merger mass divided by M_{BH} in GM2SI1 and GM3SI1 is 0, indicating delayed merging in SIDM. The sharp jumps in $M_{\text{merger}} / M_{\text{BH}}$ are due to merger events. The smooth decreasing seen is due to smooth accretion in M_{BH} .

(5). The bottom panel of Fig. 8 shows M_{merger} , the mass of the SMBH acquired through mergers divided by the total SMBH mass versus cosmic time. We define the SMBH merger mass to be the total SMBH mass minus the seed mass minus the mass acquired through accretion. This panel clearly shows that SIDM SMBH mergers are delayed by billions of years compared to their CDM counterparts. This merger growth also translates to the sharp jumps present in the top panel of Fig. 8. Merger rates can be influenced by the total number of SMBHs formed (halo occupation fraction), or by decreased dynamical friction due to SIDM as found in Di Cintio et al. (2017). Here we demonstrate that the merger rates are correlated with the number of SMBHs that have formed in our simulations, see Fig. 4. However, decreased dynamical friction also likely further delays SMBH growth in the SIDM galaxies. The main SMBHs of the largest progenitors in our CDM runs subsequently acquire large boosts in SMBH mass from increased merging. The increased growth in the CDM SMBHs due

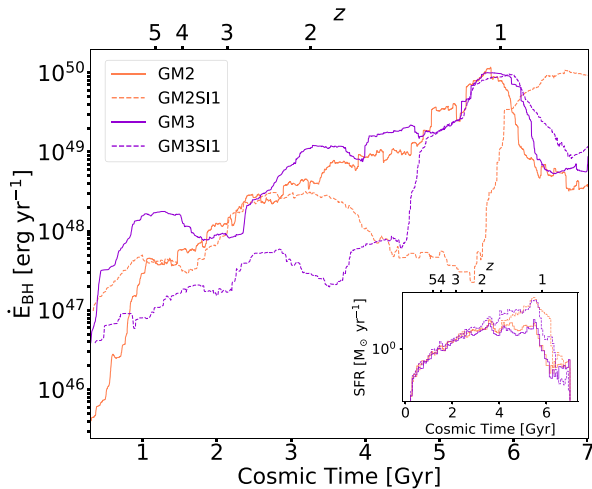


Figure 9. Rate of energy injected from the most massive SMBH (\dot{E}_{BH}) of the major progenitors in each simulation at $z = 0$ versus cosmic time. Same colour-scheme as previous figures. In the GM3-suite there is a large offset between GM3 and GM3S11 for $t < 4.5$, whereas in the GM2-suite the injected SMBH energy in GM2 surpasses the GM2S11 SMBH starting at $t = 3$ Gyr, with the difference growing out to 6 Gyr. The SMBH energy injected is correlated with the SFR of the host galaxies in all four simulations. Inset: Log of SFR versus cosmic time in all four simulations to compare with \dot{E}_{BH} .

to merging will have large effects on the subsequent evolution of our CDM simulated galaxies, as SMBH accretion is proportional to M_{BH}^2 .

SMBH accretion has been linked with regulating star formation in MW-mass galaxies (Silk & Rees 1998; Di Matteo et al. 2005; Croton et al. 2006) as SMBH accretion produces feedback which can heat up and displace gas from the central regions of galaxies (and large fractions of the star forming disc region of galaxies). The suppressed SMBH–SMBH merger rate in the SIDM galaxies relative to the CDM galaxies causes their central SMBHs to grow through mergers less efficiently. In the Bondi formalism, a lower mass SMBH accretes less mass than a more massive counterpart, therefore the SMBHs in the SIDM run have suppressed accretion with respect to the CDM runs. The suppressed SMBH accretion further suppresses SMBH feedback, thus regulating star formation less effectively in the SIDM galaxies relative to the CDM galaxies. This results in a larger production of stars in the SIDM galaxies compared to the CDM galaxies. This can be seen by examining Fig. 9.

Starting with the GM2-Suite we see that from $t = 0.5$ –1 Gyr, the energy injected from the central SMBHs is greater in the SIDM galaxy, compared to the CDM galaxy, however star formation is small compared to the mean SFR during this epoch and thus is unaffected by this difference. From $t \approx 1$ –3 Gyr the SMBH energy injected is comparable in GM2 and GM2S11 and the star formation in the two galaxies is very similar. At $t = 3$ Gyr, the energy injected from GM2 starts to increase relative to GM2S11 and the difference in injected energy continues to grow to $t = 5.5$ Gyr. A gigayear after the two SMBHs start to deviate in injected SMBH energy, GM2S11 starts to produce more stars compared to GM2 and continues to produce more stars until both galaxies quench near $t \approx 6$ Gyr.

Differences in the GM3-suite are more apparent starting from $t = 0.5$ Gyr. There is a large difference in energy injected from GM3 and GM3S11 from $t = 0.5$ –5 Gyr. These differences can be traced in the SFH. Again, at early times star formation is small compared to the mean SFR, and thus it is not until $t \approx 2.5$ Gyr that

we start to see deviations in star formation in GM3S11 compared to GM3. Delayed growth of SMBHs in SIDM relative to CDM and subsequent suppressed accretion results in very different galaxies in SIDM compared to CDM even when you start with identical ICs, as can be seen in Fig. 2.

4 DISCUSSION AND CONCLUSIONS

In this study, we used fully cosmological galaxy simulations in CDM and SIDM with a constant cross-section of $1 \text{ cm}^2 \text{ g}^{-1}$ to examine how the co-evolution of SMBHs and their MW-mass host galaxies ($M_{\text{vir}} \approx 7 \times 10^{11} M_{\odot}$ at $z = 0$) is influenced by different DM models. To do this, we used physically motivated models of SMBH formation and growth (T15; T17) and simulated an MW-mass galaxy with quenched star formation in CDM and SIDM to maximize the effects of SMBH growth on galaxy evolution. We then ran a genetically modified (Roth et al. 2016) version of these galaxies to check for result dependent sensitivity to small changes. We found that

- (i) SMBH formation is consistently suppressed in SIDM relative to a classic Λ CDM cosmology. Our CDM simulations produced about 2 or 3 times as many SMBHs compared to our SIDM simulations.
- (ii) SIDM delays SMBH growth through mergers by billions of years compared to CDM growth.
- (iii) SIDM SMBHs generate less SMBH feedback compared to CDM SMBHs during the first 5 Gyr of their evolution. Nonetheless, by $z = 0.8$ their SMBH masses differ only by around 0.2 dex, so that both CDM and SIDM runs remain compatible with the $M_{\text{BH}}-M_*$ relation (Schramm & Silverman 2013).
- (iv) SIDM galaxies have a larger central reservoir of gas available for star formation.
- (v) SIDM galaxies form about 3 or 4 times more stars than CDM galaxies over their lifetimes.

Importantly, Di Cintio et al. (2017) also finds less massive SMBHs and more stars in their MW-mass galaxies from abundance matching at a much higher SIDM cross-section of $\sigma_{\text{dm}} = 10 \text{ cm}^2 \text{ g}^{-1}$. At lower masses, the effects of delayed SMBH growth should not matter much given that SMBHs grow very little in dwarf galaxies (Volonteri, Lodato & Natarajan 2008; Habouzit, Volonteri & Dubois 2017; Bellovary et al. 2019). SMBHs are thus not expected to have a significant impact in regulating star formation in dwarf galaxies (but see Silk 2017; Sharma et al. 2019). In particular, at $z > 2$, or equivalently for a given halo mass less than MW-mass, the largest progenitors of our main $z = 0$ galaxies have stellar masses that agree to within 0.3 dex, the typical scatter of the stellar mass–halo mass relation. In both models the stellar masses at a given halo mass are higher than those found in Behroozi, Wechsler & Conroy (2013). However, for $z < 2$ the stellar masses at a given halo mass deviate well beyond the 0.3 dex scatter. The large difference at low redshift may thus be used in a future study with a larger statistical sample to distinguish the two DM models.

It should be noted that, similar to Di Cintio et al. (2017), these simulations do not have high enough resolution to produce dark matter cores in CDM due to bursty SNe feedback. However this will not significantly alter the results of this study. There is not enough star formation in the CDM galaxies during the epoch of SMBH formation to produce cores since these galaxies have stellar mass less-than or equal to $10^6 M_{\odot}$, the threshold for star formation to start to core DM haloes (see fig. 7 of Governato et al. 2015). At late times, baryons dominate the central regions of MW-mass galaxies,

dramatically shrinking cores formed in SIDM (Di Cintio et al. 2014b; Kaplinghat et al. 2014).

Despite the fact that our simulations include well-motivated models of SMBH formation and growth, they are still relatively simple subgrid models. Further, our SMBH subgrid parameters are based on matching observations at $z = 0$ in a Λ CDM cosmology and thus future work requires an investigation of how and if these parameters might be altered if instead matched to Λ SIDM. On the other hand, both CDM and SIDM runs remain compatible with the $z = 0.8 M_{\text{BH}}-M_*$ relationship found in Schramm & Silverman (2013), thus indicating that SIDM does not demand a re-calibration of feedback. Further, in terms of SMBH seeding parameters, most SMBH formation models require high density, very low metallicity gas with similar threshold values to those used in this work (see Volonteri 2012). Future work requires a larger simulation with higher output resolution to more thoroughly quantify how SIDM influences gas densities at high- z . However, based on the tests conducted in this work, our hypothesis that SIDM lowers central gas densities due to self-interactions at high- z holds. Thus, given our limitations and small sample size, this study is a useful case study which shows that, given a well-motivated SMBH formation prescription, SIDM can significantly alter SMBH merger histories and delay growth and feedback which results in very different galaxy evolution of MW-mass objects compared to the classic Λ CDM model.

ACKNOWLEDGEMENTS

For our simulation analysis we utilized PYNBODY (Pontzen et al. 2013) and TANGOS (Pontzen & Tremmel 2018). This material is based upon work supported by the National Science Foundation Graduate Research Fellowship under Grant No. DGE-1762114. AC would like to thank Matt McQuinn, Vid Irsic, Jessica Werk, Annika Peter, Charlotte Christensen, Iryna Butsky, Jillian Belovary, Ray Sharma, and Sarah Loebman for useful conversations through out the progression of this work. We would also like to give special thanks to the thoughtful and informative comments from our referee. ADC acknowledges financial support from a Marie-Sklodowska-Curie Individual Fellowship grant, H2020-MSCA-IF-2016 Grant agreement 748213, DIGESTIVO. AP was supported by the Royal Society. Resources supporting this work were provided by the NASA High-End Computing (HEC) Program through the National Aeronautics and Space Administration Advanced Supercomputing (NAS) Division at Ames Research Center. This work used the Extreme Science and Engineering Discovery Environment (XSEDE), which is supported by National Science Foundation grant number ACI-1548562. This work has received funding from the European Union's Horizon 2020 research and innovation programme under grant agreement No. 818085 GMGalaxies.

DATA AVAILABILITY

The data for this research was generated from a proprietary branch of CHANGA which is available on github (<http://github.com/N-BodyShop/changa>). Analysis was conducted using the publicly available software PYNBODY (Pontzen et al. 2013, <https://github.com/pynbody/pynbody>) and TANGOS (Pontzen & Tremmel 2018, <https://github.com/pynbody/tangos>). The results in this work were generated from the Pioneer GM cosmological simulations. The raw outputs of these simulations can be accessed upon request from Akaxia Cruz (admcruz@uw.edu), along with the TANGOS data base files that were generated from these simulation outputs and directly used for this analysis.

REFERENCES

- Adams J. J. et al., 2014, *ApJ*, 789, 63
 Balberg S., Shapiro S. L., Inagaki S., 2002, *ApJ*, 568, 475
 Bastidas Fry A. et al., 2015, *MNRAS*, 452, 1468
 Behroozi P. S., Wechsler R. H., Conroy C., 2013, *ApJ*, 770, 57
 Belovary J. M., Governato F., Quinn T. R., Wadsley J., Shen S., Volonteri M., 2010, *ApJ*, 721, L148
 Belovary J. M., Cleary C. E., Munshi F., Tremmel M., Christensen C. R., Brooks A., Quinn T. R., 2019, *MNRAS*, 482, 2913
 Benítez-Llambay A., Frenk C. S., Ludlow A. D., Navarro J. F., 2019, *MNRAS*, 488, 2387
 Binney J., Tremaine S., 2008, *Galactic Dynamics*, 2nd edn. Princeton Univ. Press, Princeton
 Booth C. M., Schaye J., 2009, *MNRAS*, 398, 53
 Boylan-Kolchin M., Ma C.-P., Quataert E., 2008, *MNRAS*, 383, 93
 Breddels M. A., Helmi A., van den Bosch R. C. E., van de Ven G., Battaglia G., 2013, *MNRAS*, 433, 3173
 Brooks A. M., Zolotov A., 2014, *ApJ*, 786, 87
 Bullock J. S., Kolatt T. S., Sigad Y., Somerville R. S., Kravtsov A. V., Klypin A. A., Primack J. R., Dekel A., 2001, *MNRAS*, 321, 559
 Burkert A., 2000, *ApJ*, 534, L143
 Castignani G., Frusciante N., Vernieri D., Salucci P., 2012, preprint ([arXiv:1201.3998](https://arxiv.org/abs/1201.3998))
 Chandrasekhar S., 1943, *ApJ*, 97, 255
 Colín P., Avila-Reese V., Valenzuela O., Firmani C., 2002, *ApJ*, 581, 777
 Croton D. J. et al., 2006, *MNRAS*, 365, 11
 Cyr-Racine F.-Y., Sigurdson K., Zavala J., Bringmann T., Vogelsberger M., Frommer C., 2016, *Phys. Rev. D*, 93, 123527
 D'Onghia E., Burkert A., 2003, *ApJ*, 586, 12
 de Blok W. J. G., McGaugh S. S., 1997, *MNRAS*, 290, 533
 de Blok W. J. G., McGaugh S. S., Bosma A., Rubin V. C., 2001, *ApJ*, 552, L23
 de Blok W. J. G., Walter F., Brinks E., Trachternach C., Oh S. H., Kennicutt R. C. J., 2008, *AJ*, 136, 2648
 Di Cintio A., Brook C. B., Macciò A. V., Stinson G. S., Knebe A., Dutton A. A., Wadsley J., 2014a, *MNRAS*, 437, 415
 Di Cintio A., Brook C. B., Dutton A. A., Macciò A. V., Stinson G. S., Knebe A., 2014b, *MNRAS*, 441, 2986
 Di Cintio A., Tremmel M., Governato F., Pontzen A., Zavala J., Fry A. B., Brooks A., Vogelsberger M., 2017, *MNRAS*, 469, 2845
 Di Matteo T., Springel V., Hernquist L., 2005, *Nature*, 433, 604
 Elbert O. D., Bullock J. S., Kaplinghat M., Garrison-Kimmel S., Graus A. S., Rocha M., 2018, *ApJ*, 853, 109
 Firmani C., D'Onghia E., Chincarini G., Hernández X., Avila-Reese V., 2001, *MNRAS*, 321, 713
 Flores R. A., Primack J. R., 1994, *ApJ*, 427, L1
 Garrison-Kimmel S. et al., 2019, *MNRAS*, 487, 1380
 Gentile G., Salucci P., Klein U., Vergani D., Kalberla P., 2004, *MNRAS*, 351, 903
 Gnedin O. Y., Ostriker J. P., 2001, *ApJ*, 561, 61
 Governato F. et al., 2012, *MNRAS*, 422, 1231
 Governato F. et al., 2015, *MNRAS*, 448, 792
 Guedes J., Callegari S., Madau P., Mayer L., 2011, *ApJ*, 742, 76
 Habouzit M., Volonteri M., Dubois Y., 2017, *MNRAS*, 468, 3935
 Kahlhoefer F., Kaplinghat M., Slatyer T. R., Wu C.-L., 2019, *JCAP*, 2019, 010
 Kamada A., Kaplinghat M., Pace A. B., Yu H.-B., 2017, *Phys. Rev. Lett.*, 119, 111102
 Kaplinghat M., Keeley R. E., Linden T., Yu H.-B., 2014, *Phys. Rev. Lett.*, 113, 021302
 Kaplinghat M., Ren T., Yu H.-B., 2020, *JCAP*, 2020, 027
 Kaplinghat M., Valli M., Yu H.-B., 2019b, *MNRAS*, 490, 231
 Keller B. W., Wadsley J. W., Wang L., Kruijssen J. M. D., 2019, *MNRAS*, 482, 2244
 Knollmann S. R., Knebe A., 2009, *ApJS*, 182, 608
 Koda J., Shapiro P. R., 2011, *MNRAS*, 415, 1125
 Kroupa P., 2001, *MNRAS*, 322, 231

- Kuzio de Naray R., Spekkens K., 2011, *ApJ*, 741, L29
- Kuzio de Naray R., McGaugh S. S., de Blok W. J. G., 2008, *ApJ*, 676, 920
- Menon H., Wesolowski L., Zheng G., Jetley P., Kale L., Quinn T., Governato F., 2015, *Comput. Astrophys. Cosmol.*, 2, 1
- Moore B., 1994, *Nature*, 370, 629
- Moore B., Governato F., Quinn T., Stadel J., Lake G., 1998, *ApJ*, 499, L5
- Navarro J. F., Frenk C. S., White S. D. M., 1997, *ApJ*, 490, 493
- Nishikawa H., Boddy K. K., Kaplinghat M., 2020, *Phys. Rev. D*, 101, 063009
- Oh S.-H., de Blok W. J. G., Walter F., Brinks E., Kennicutt Robert C. J., 2008, *AJ*, 136, 2761
- Oñorbe J., Boylan-Kolchin M., Bullock J. S., Hopkins P. F., Kereš D., Faucher-Giguère C.-A., Quataert E., Murray N., 2015, *MNRAS*, 454, 2092
- Peter A. H. G., Rocha M., Bullock J. S., Kaplinghat M., 2013, *MNRAS*, 430, 105
- Planck Collaboration et al., 2014, *A&A*, 571, A16
- Pontzen A., Governato F., 2012, *MNRAS*, 421, 3464
- Pontzen A., Governato F., 2014, *Nature*, 506, 171
- Pontzen A., Tremmel M., 2018, *ApJS*, 237, 23
- Pontzen A. et al., 2008, *MNRAS*, 390, 1349
- Pontzen A., Roškar R., Stinson G., Woods R., 2013, pynbody: N-Body/SPH analysis for python, record ascl:1305.002
- Pontzen A., Tremmel M., Roth N., Peiris H. V., Saintonge A., Volonteri M., Quinn T., Governato F., 2017, *MNRAS*, 465, 547
- Power C., Navarro J. F., Jenkins A., Frenk C. S., White S. D. M., Springel V., Stadel J., Quinn T., 2003, *MNRAS*, 338, 14
- Read J. I., Gilmore G., 2005, *MNRAS*, 356, 107
- Ren T., Kwa A., Kaplinghat M., Yu H.-B., 2019, *Phys. Rev. X*, 9, 031020
- Ritchie B. W., Thomas P. A., 2001, *MNRAS*, 323, 743
- Robertson A., Massey R., Eke V., Bower R., 2015, *MNRAS*, 453, 2267
- Robertson A., Massey R., Eke V., 2017, *MNRAS*, 465, 569
- Robles V. H. et al., 2017, *MNRAS*, 472, 2945
- Rocha M., Peter A. H. G., Bullock J. S., Kaplinghat M., Garrison-Kimmel S., Oñorbe J., Moustakas L. A., 2013, *MNRAS*, 430, 81
- Roth N., Pontzen A., Peiris H. V., 2016, *MNRAS*, 455, 974
- Salucci P., Wilkinson M. I., Walker M. G., Gilmore G. F., Grebel E. K., Koch A., Frigerio Martins C., Wyse R. F. G., 2012, *MNRAS*, 420, 2034
- Sanchez N. N., Werk J. K., Tremmel M., Pontzen A., Christensen C., Quinn T., Cruz A., 2019, *ApJ*, 882, 8
- Santos-Santos I. M., Di Cintio A., Brook C. B., Macciò A., Dutton A., Domínguez-Tenreiro R., 2018, *MNRAS*, 473, 4392
- Santos-Santos I. M. E. et al., 2020, *MNRAS*, 495, 58
- Schaye J. et al., 2015, *MNRAS*, 446, 521
- Schramm M., Silverman J. D., 2013, *ApJ*, 767, 13
- Sharma R., Brooks A., Somerville R. S., Tremmel M., Bellovary J., Wright A., Quinn T., 2020, *ApJ*, 897, 103
- Shen S., Wadsley J., Stinson G., 2010, *MNRAS*, 407, 1581
- Sijacki D., Springel V., Di Matteo T., Hernquist L., 2007, *MNRAS*, 380, 877
- Silk J., 2017, *ApJ*, 839, L13
- Silk J., Rees M. J., 1998, *A&A*, 331, L1
- Simon J. D., Bolatto A. D., Leroy A., Blitz L., Gates E. L., 2005, *ApJ*, 621, 757
- Spergel D. N., Steinhardt P. J., 2000, *Phys. Rev. Lett.*, 84, 3760
- Stinson G., Seth A., Katz N., Wadsley J., Governato F., Quinn T., 2006, *MNRAS*, 373, 1074
- Taffoni G., Mayer L., Colpi M., Governato F., 2003, *MNRAS*, 341, 434
- Tollet E. et al., 2016, *MNRAS*, 456, 3542
- Tremmel M., Governato F., Volonteri M., Quinn T. R., 2015, *MNRAS*, 451, 1868
- Tremmel M., Karcher M., Governato F., Volonteri M., Quinn T. R., Pontzen A., Anderson L., Bellovary J., 2017, *MNRAS*, 470, 1121
- Tremmel M., Governato F., Volonteri M., Quinn T. R., Pontzen A., 2018a, *MNRAS*, 475, 4967
- Tremmel M., Governato F., Volonteri M., Pontzen A., Quinn T. R., 2018b, *ApJ*, 857, L22
- Tremmel M. et al., 2019, *MNRAS*, 483, 3336
- Vogelsberger M., Zavala J., 2013, *MNRAS*, 430, 1722
- Vogelsberger M., Zavala J., Loeb A., 2012, *MNRAS*, 423, 3740
- Vogelsberger M., Zavala J., Simpson C., Jenkins A., 2014, *MNRAS*, 444, 3684
- Vogelsberger M., Zavala J., Cyr-Racine F.-Y., Pfrommer C., Bringmann T., Sigurdson K., 2016, *MNRAS*, 460, 1399
- Volonteri M., 2012, *Science*, 337, 544
- Volonteri M., Lodato G., Natarajan P., 2008, *MNRAS*, 383, 1079
- Wadsley J. W., Stadel J., Quinn T., 2004, *New Astron.*, 9, 137
- Wadsley J. W., Veeravalli G., Couchman H. M. P., 2008, *MNRAS*, 387, 427
- Wadsley J. W., Keller B. W., Quinn T. R., 2017, *MNRAS*, 471, 2357
- Walker M. G., Peñarrubia J., 2011, *ApJ*, 742, 20
- Wechsler R. H., Bullock J. S., Primack J. R., Kravtsov A. V., Dekel A., 2002, *ApJ*, 568, 52
- Yoshida N., Springel V., White S. D. M., Tormen G., 2000, *ApJ*, 544, L87
- Zavala J., Vogelsberger M., Walker M. G., 2013, *MNRAS*, 431, L20
- Zavala J., Lovell M. R., Vogelsberger M., Burger J. D., 2019, *Phys. Rev. D*, 100, 063007

This paper has been typeset from a $\text{\TeX}/\text{\LaTeX}$ file prepared by the author.